Dalton Transactions

PAPER

View Article Online
View Journal | View Issue

Cite this: *Dalton Trans.*, 2014, **43**, 13865

$CoMn_2O_4$ hierarchical microspheres with high catalytic activity towards *p*-nitrophenol reduction†

Xiaohui Shi,[a] Fangcai Zheng,[a] Nan Yan[a] and Qianwang Chen*[a,b]

Received 7th June 2014,
Accepted 28th July 2014

DOI: 10.1039/c4dt01686f

www.rsc.org/dalton

The $CoMn_2O_4$ hierarchical microspheres assembled by nanosheets through thermal decomposition of the precursor at different temperatures were first used as catalysts in the reduction of *p*-nitrophenol to *p*-aminophenol. The sample prepared at 500 °C shows the highest catalytic activity (k_{app} 14.95 × 10^{-3} s^{-1}), which is even higher than some results reported for noble metal particles (Au, Ag and Pd). It is suggested that the presence of metal oxide with 'd^7' (Co element) and 'd^5' (Mn element) electronic configurations and the special morphology of $CoMn_2O_4$ hierarchical microspheres are beneficial to the reduction of *p*-nitrophenol to *p*-aminophenol.

Introduction

About 90% of all commercially produced chemical products involve catalysts at some stage in the process of their preparation; catalytic hydrogenation of *p*-nitrophenol is one of the most studied catalytic reactions, because *p*-nitrophenol is one of the most refractory pollutants, while *p*-aminophenol is an important intermediate in the manufacture of pharmaceuticals such as paracetamol, acetanilide, phenacetin *etc.*[1–3] *p*-Aminophenol is also used in large amounts as a photographic developer, corrosion inhibitor, anticorrosion-lubricant and hair-dyeing agent.[4–6] Therefore, it is important to develop a green and cheap catalyst for catalytic hydrogenation of *p*-nitrophenol.

As the major catalysts used in catalytic hydrogenation of *p*-nitrophenol, noble metal nanoparticles have attracted the attention of researchers for a long time. Noble metal nanoparticles such as Pd, Pt, Rh, Ru and Au have been widely studied in hydrogenation and oxidation reactions.[7–10] Metal oxide supported noble metal nanoparticles have also been tested as catalysts for the reduction of *p*-nitrophenol to *p*-aminophenol in the presence of $NaBH_4$. For example, Pd nanoparticles dispersed on the alumina substrate have been reported.[11] Taekyung *et al.* prepared PVP-stabilized Pt nanoparticles and CeO_2 supported Pt nanoparticles as catalysts in the reaction,[12] PVP-stabilized Pt nanoparticles show higher activity than the Pt/CeO_2 compound; however, they lose their catalytic activities upon recycling. Gold coated Fe_3O_4 has also been used as a catalyst in the reaction.[13] Although the noble metal catalysts display outstanding properties, it is often the case that a sudden drop in catalytic activity is observed after the catalytic transformation due to the aggregation and leaching of the noble metal catalysts.[14] For example, it is found that a smaller AuNP tends to show a higher catalytic activity as it has a much greater surface to volume ratio.[15] However, smaller AuNPs easily aggregate to minimize their surface area due to their higher surface energy, resulting in a remarkable reduction in their catalytic activities.[16] Some researchers try to solve this problem through introducing SiO_2 shells;[12] in such an approach, it can prevent their aggregation to a large degree, but the preparation is time consuming due to its complex procedure. On the other hand, relatively expensive in terms of manufacturing cost was the common disadvantage of these catalysts, which is obvious and inevitable. These problems cause severe restrictions in using costly metal nanoparticles as catalysts for large scale applications. Hence, more and more attention has been paid to non-noble metal catalysts, such as carbon materials,[17,18] transition metals[19,20] and metal oxides.[21]

Metal oxides with higher reactivity along with other advantages such as thermal stability, chemical stability, easy recovery and reusability may become promising cost effective catalysts and have been explored in recent years. Metal oxides, especially spinel type composite metal oxides of the general formula AB_2O_4 containing 3d metal ions, have been investigated as catalysts for many organic catalytic reactions.[22] For example, the photocatalytic activity of CuM_2O_4 (M = Al, Cr, Mn, Fe and Co) was explored for the evolution of H_2.[23] The catalytic activity of $NiFe_2O_4$ for one-step hydroxylation of benzene into phenol has also been studied in-depth by

[a]*Hefei National Laboratory for Physical Sciences at Microscale, Department of Materials Science & Engineering & Collaborative Innovation Center of Suzhou Nano Science and Technology, University of Science and Technology of China, Hefei, China. E-mail: cqw@ustc.edu.cn*

[b]*High Magnetic Field Laboratory, Hefei Institutes of Physical Science, Chinese Academy of Sciences, Hefei, China. E-mail: cqw@ustc.edu.cn; Fax: +86 551 63603005; Tel: +86 551 63603005*

†Electronic supplementary information (ESI) available. See DOI: 10.1039/c4dt01686f

Ibraheem Othman Ali.[24] T. Mathew used $Cu_{0.5}Co_{0.5}Fe_2O_4$ as a catalyst to synthesize orthoalkyl phenols.[25] Though the high catalytic performance of metal oxide supported noble metal catalysts has been reported in the literature, there are only a few reports regarding the use of metal oxides as catalysts in the catalytic hydrogenation of *p*-nitrophenol. Triveni Rajashekhar Mandlimath investigated the catalytic activities of the first row transition metal oxides in the conversion of *p*-nitrophenol to *p*-aminophenol.[21] Importantly, it has been proved the metal oxides possessing the 'd^n' (n = 5–9) electronic configuration are active catalysts because the 'd^n' configuration can induce the catalytic reduction by relaying electrons from the donor BH_4^- ions to the acceptor once they get adsorbed on the surface of metal oxides. It is worth noting that complex oxides with a spinel structure are found to be promising catalysts on account of their better activity and thermal stability as compared to individual oxides.[26] As a typical complex oxide, $CoMn_2O_4$ exhibits a variety of applications in electronics, magnetic materials and catalysts,[27–29] and importantly, we noticed that this metal oxide possesses 'd^7' (Co element) and 'd^5' (Mn element) electronic configurations that are active in the reduction of *p*-nitrophenol to *p*-aminophenol. In general, redox couples (Co^{3+}/Co^{2+} and Mn^{3+}/Mn^{2+}) can form in the preparation of this spinel oxide. An effective catalyst with an intermediate redox potential value of the donor–acceptor partner helps in electron transfer and acts as an electron relay system.[30] Therefore, it is suggested that $CoMn_2O_4$ can possibly show high activity in the catalytic hydrogenation of *p*-nitrophenol. Here, we report the preparation and catalytic hydrogenation of *p*-nitrophenol with $CoMn_2O_4$. The reaction mechanism over $CoMn_2O_4$ hierarchical microspheres is also discussed.

Experimental section

Synthesis

All of the reagents used are of analytical purity and used without further purification. The precursor for preparing $CoMn_2O_4$ hierarchical microspheres were synthesized according to our previous report.[27] In a typical synthesis process, 1 mmol Mn $(CH_3COO)_2{\cdot}4H_2O$ (0.245 g), 0.5 mmol Co-$(CH_3COO)_2{\cdot}4H_2O$ (0.124 g) and 1 g polyethylene glycol 1000 were dissolved in 35 ml ethylene glycol to form a clear solution. After being stirred vigorously for 10 min, the mixture was put into a 50 ml Teflon-lined stainless steel autoclave. The autoclave was heated at 200 °C and maintained for 6 h before being cooled in air. The resulting precipitate was then centrifuged, washed with distilled water and ethanol and then dried in an oven at 60 °C. The thermal decomposition of the purple precursor of $CoMn_2O_4$ was performed at 400 °C, 500 °C, 600 °C and 700 °C, respectively, for 3 h in air in the oven at a heating rate of 10 °C min^{-1}.

Characterization

The powder X-ray diffraction (XRD) patterns were collected on a Japan Rigaku D/MAX-cA X-ray diffractometer equipped with Cu Kα radiation over the 2θ range of 20–80°. Scanning electron microscopy (SEM) images were obtained on a JEOL JSM-6700M scanning electron microscope. X-ray photoelectron spectroscopy (XPS) was performed on an ESCALAB 250 X-ray Photoelectron Spectrometer with Al Kα radiation. The UV-vis absorption spectra were recorded on an UV-vis spectrophotometer (TU-1810, Beijing).

Catalytic performance measurements

The reaction proceeded under ambient conditions. Typically, the catalytic reactions were conducted by mixing 200 μl *p*-nitrophenol aqueous solution (1 mM) with 200 μl freshly prepared $NaBH_4$ aqueous solution (0.1 M) in a quartz cuvette, and then adding 2.5 ml deionized water to the quartz cuvette and gently shaking to mix them evenly. Subsequently, 100 μl $CoMn_2O_4$ aqueous suspension (1.4 mg ml^{-1}) was injected to the above reaction mixture to start the reduction, which was monitored using UV-vis spectroscopy over a scanning range of 200–500 nm. The rate constant of the reaction was measured by the extinction of the solution at 400 nm as a function of time and the decrease in absorbance at 400 nm was recorded at 0.5 s intervals by time scanning of the UV spectrometer.

Results and discussion

XRD analysis

The synthesis includes two steps, preparation of a $CoMn_2O_4$ precursor by a hydrothermal process and then thermal conversion to $CoMn_2O_4$ at different temperatures. The structure of the samples after calcining was analyzed by X-ray powder diffraction (XRD); as shown in Fig. 1, all peaks from the four samples can be well indexed as spinel $CoMn_2O_4$ (JCPDS: 77-0471). The sharpening of the peaks is observed with increase in the calcination temperature, indicating the improvement in crystalline quality. The mean crystallite sizes are estimated from the (211) peak with the Scherrer formula,

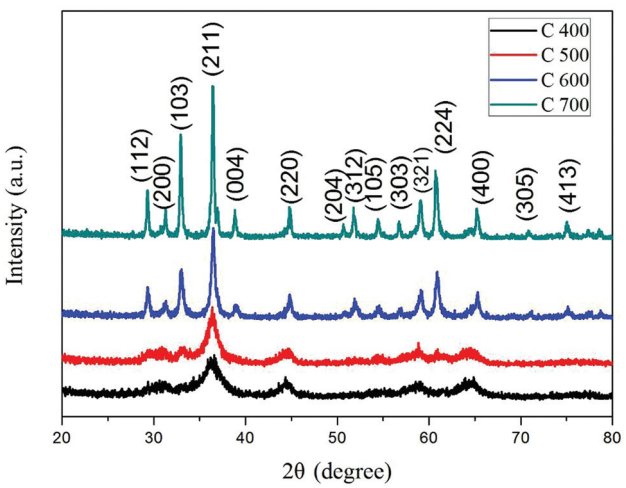

Fig. 1 XRD patterns of $CoMn_2O_4$ hierarchical microspheres prepared at different temperatures.

$D = 0.89\lambda/(B\cos\theta)$ (D, average dimension of crystallites; λ, the X-ray wavelength; B, the pure diffraction broadening of a peak at half-height; θ, the Bragg angle). The sizes are 6.08 nm, 6.65 nm, 18.28 nm and 30.85 nm for the samples at different thermal decomposition temperatures from C400 to C700, respectively. The minimization tendency of the interfacial surface energy is considered to be the major driving force for crystallite growth during the annealing process.[31–33] $CoMn_2O_4$ hierarchical microspheres were prepared at different calcination temperatures to reveal the impact of crystalline quality and particle size on the catalytic performance, which will be discussed in the following sections.

SEM analysis

The morphologies of the $CoMn_2O_4$ hierarchical microspheres were examined by scanning electron microscopy (SEM). Fig. 2 shows the images of $CoMn_2O_4$ hierarchical microspheres obtained at different sintering temperatures. Fig. 2(a) shows the product thermal decomposition at 400 °C, hierarchical microspheres with uniform size and shape are clearly observed, these microspheres are assembled by nanosheets without serious aggregation. The morphologies of C500, C600 and C700, shown in Fig. 2, do not show much difference compared with C400.

XPS analysis

XPS measurements were carried out to further determine the chemical composition of as-prepared $CoMn_2O_4$ hierarchical microspheres prepared at different thermal decomposition temperatures. The binding energy (BE) was corrected for specimen charging by referencing them to the C 1s peak (set at 284.6 eV). As shown in Fig. 3(a), all the samples show a similar feature with the two peaks of Co 2p centered at 780.7 and 795.7 eV, respectively, the gap between the two peaks is about 15 eV (spin–orbit splitting), which corresponds to Co^{2+} and Co^{3+}.[34] However, with the increase in the thermal decomposition temperature the left shift of Mn $2p_{3/2}$ peak located at 642.0 eV was observed. Fig. 3(b) showed the Mn 2p spectra of the four samples, each sample has two peaks around 642.0 (Mn $2p_{3/2}$) and 653.5 eV (Mn $2p_{1/2}$). It is noted that the precise location of the four samples were 642.2 (C400), 642.1 (C500), 642.0 (C600) and 641.9 eV (C700), respectively, which shows that there is an obvious left shift trend. In order to manifest the cause of the change, we took C500 as an example, the Mn 2p spectrum features two main spin–orbit lines of $2p_{3/2}$ at ~642.0 eV and $2p_{1/2}$ at ~653.5 eV with a separation of 11.5 eV (Fig. 3(d)) (the Mn 2p spectrum features of C400, C600 and C700 are shown in Fig. S1†). Using a Gaussian-fitting method, a small satellite structure could be observed. After refined-fitting, the spectrum can be deconvolved into four peaks. Among them, 641.5 and 653.0 eV can be assigned to Mn(II), while other two peaks at 642.9 and 653.7 eV are characteristics of Mn(III).[35] According to the previous analysis, the left shift trend suggests that the ratio of Mn^{3+} (642.9 eV and 653.7 eV) was increased with an increase in calcination temperature (Table 1). Therefore, it is concluded that the Mn element exists as Mn^{2+} and Mn^{3+} in these catalysts, and the calcination temperature can affect the valence-state distribution of Mn. Though the Co element also exists as two valence states (Co^{2+} and Co^{3+}) in these catalysts, the two peaks of Co $2p_{3/2}$ and Co $2p_{1/2}$ located at 780.2 and 795.7 eV showed no significant change in these catalysts.

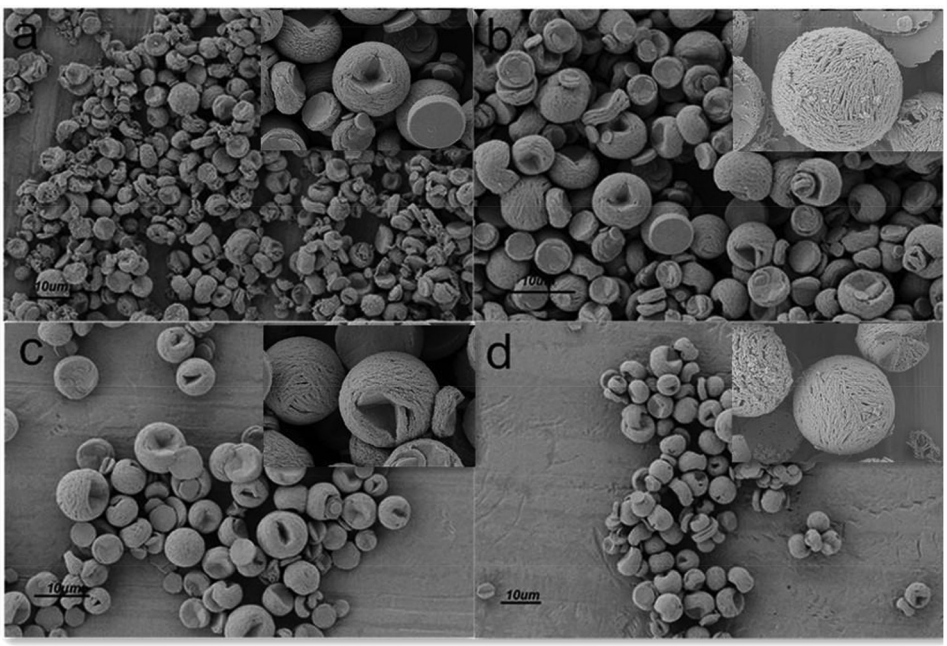

Fig. 2 SEM images of $CoMn_2O_4$ hierarchical microspheres prepared at different temperatures, C400, C500, C600 and C700 (a–d), respectively.

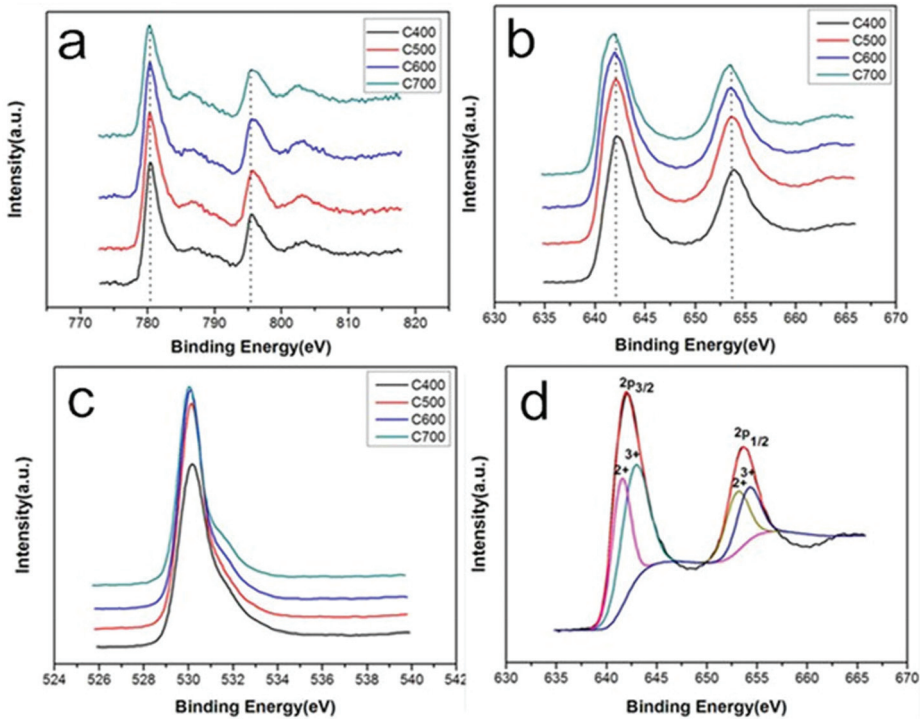

Fig. 3 XPS survey spectra of $CoMn_2O_4$ hierarchical microspheres: (a) Co 2p, (b) Mn 2p, (c) O 1s, (d) Mn 2p of C500.

Table 1 The ratio of Mn^{3+}/Mn^{2+} in the products based on the area of peaks after a Gaussian fitting method

Sample	The ratio of Mn^{3+}/Mn^{2+}
C400	0.95
C500	1.15
C600	1.67
C700	2.08

Catalytic reduction of *p*-nitrophenol

The catalytic reduction of *p*-nitrophenol to *p*-aminophenol in the presence of an excess amount of $NaBH_4$ was chosen to investigate the catalytic activity of the catalysts (C400, C500, C600 and C700). For all the experiments, the initial concentrations of *p*-nitrophenol and $NaBH_4$ were kept at 1 mM and 0.1 M, respectively. Fig. 4 shows the typical UV-vis spectra of absorbance change of *p*-nitrophenol in the presence of $NaBH_4$ and different catalysts (C400, C500, C600 and C700). Without the addition of $CoMn_2O_4$ hierarchical microspheres, the absorption band of *p*-nitrophenol (l_{max} $\frac{1}{4}$ 317 nm) is red shifted to 400 nm due to the formation of *p*-nitrophenolate ions under alkaline conditions by the introduction of $NaBH_4$, indicated by the color change from light yellow to dark yellow after addition of $NaBH_4$. The absorption peak at 400 nm remained unaltered for a long period of time without the presence of $CoMn_2O_4$ hierarchical microsphere catalysts, which implies that *p*-nitrophenolate anions cannot be reduced by aqueous $NaBH_4$.[36] While, when a small amount of $CoMn_2O_4$ hierarchical microsphere catalyst (C400) was added to the solution at room temperature (18 °C), no change in the absorbance of *p*-nitrophenol was observed within the first 3 min, which we define as the induction period (t_0).

After the induction period, the reaction starts, the dark yellow color of *p*-nitrophenol solution vanished quickly, indicated by the fast decrease in the absorbance of 400 nm. Concomitantly, a new peak appeared at 300 nm, and increased with reduction in time, which is assigned to *p*-aminophenol, confirming the reduction of *p*-nitrophenol to *p*-aminophenol. In addition, GC-MS analysis also showed that all of the *p*-nitrophenol was converted to *p*-aminophenol after the reaction (Fig. S2†). The same spectral changes of reducing *p*-nitrophenol were also observed for other three samples C500, C600 and C700, as shown in Fig. 4. These results indicated that $CoMn_2O_4$ hierarchical microspheres play an important role in this reaction. Compared to the other three samples (C400, C600 and C700), C500 shows the shortest time for transforming *p*-nitrophenol to *p*-aminophenol as shown in Fig. 4. The order of the catalytic activity for the four products is C500 > C600 > C400 > C700. As an excess of $NaBH_4$ was used, the BH_4^- concentration can be considered as a constant throughout the reaction.

To compare the catalytic activity of the as-prepared $CoMn_2O_4$ hierarchical microspheres with other results reported in the literature, the apparent rate constant (k_{app}) values were calculated from Fig. 4 and shown in Table 2. The rate constant for C500 is 14.95×10^{-3} s^{-1}, as shown in Table 3 the catalytic activity of the $CoMn_2O_4$ hierarchical microspheres in our experiments is much higher than that of some Ag, Au and Pd nanoparticles for the catalytic reduction of *p*-nitro-

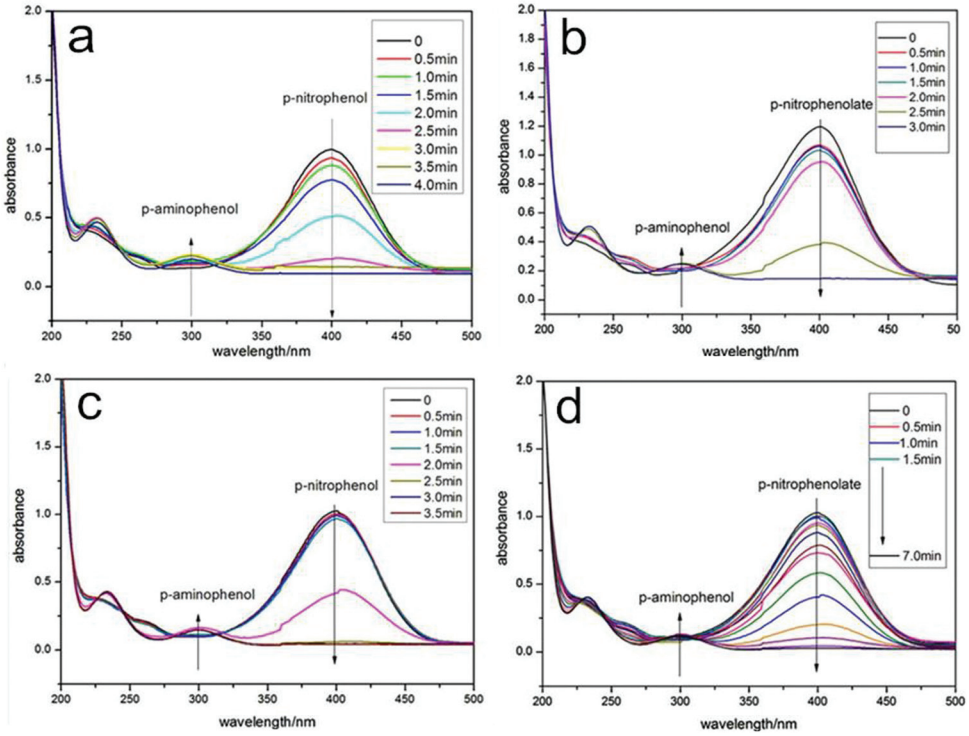

Fig. 4 (a–d) UV-vis absorption spectra of *p*-nitrophenol reduction with $NaBH_4$ catalyzed by different samples of $CoMn_2O_4$ hierarchical microspheres at room temperature, as there was no change in the absorbance of *p*-nitrophenol within the induction period (t_0), the spectrum overlapped during this time. For the clear expression of reaction time, the introduction time has not been showed in the figure: (a) C400, (b) C500, (c) C600, (d) C700 at room temperature (18 °C).

Table 2 Summary of the catalytic activity for the reduction of *p*-nitrophenol with $NaBH_4$ catalyzed by $CoMn_2O_4$ hierarchical microspheres prepared at different temperatures. The catalytic reactions were carried out at room temperature (18 °C)

Sample	$CoMn_2O_4$/mg	k_{app}/s^{-1}
C400	0.14	8.13×10^{-3}
C500	0.14	14.95×10^{-3}
C600	0.14	12.5×10^{-3}
C700	0.14	7.42×10^{-3}

k_{app} = apparent rate constant.

phenol by $NaBH_4$, except the result from bimetal catalysts reported by Zhang. It is worth noting that the quantity of $CoMn_2O_4$ hierarchical microspheres used in our experiments was approximately 2–5 orders of magnitude lower than that of the other results (except Li *et al.*); higher apparent rate constants were obtained, displaying a high catalytic activity of the $CoMn_2O_4$ hierarchical microspheres in the catalytic reduction of *p*-nitrophenol by $NaBH_4$. Moreover, the simple and low fabrication cost of $CoMn_2O_4$ hierarchical microspheres makes it a good substitute for noble metals in catalytic hydrogenation of *p*-nitrophenol.

In order to further characterize the catalytic performance of $CoMn_2O_4$ hierarchical microspheres, four types of catalysts (C400, C500, C600 and C700) were selected to investigate their reusability. After the reaction, 200 μl *p*-nitrophenol aqueous solution (1 mM) was added to the reaction solution. The change of adsorption intensity at 400 nm indicates the consumption of *p*-nitrophenol; the reduction reaction of *p*-nitrophenol was monitored by the UV-vis spectra. Rates of *p*-nitrophenol reduction and changes in the concentration of

Table 3 A comparison of rate constant for the catalytic reduction of *p*-nitrophenol by $NaBH_4$ by noble metal particle and $CoMn_2O_4$ hierarchical microspheres of this work

Entry	Catalyst	Type	Concentration of *p*-NP	Amount of catalyst	Apparent rate constant	References
1	$PPy/TiO_2/Pd$	Nanofibers	1.05×10^{-4} M	113 nmol	12.2×10^{-3} s^{-1}	37
2	Al_2O_3/Pd	Satellites–core	1.10×10^{-4} M	0.20–6.86 nmol	11×10^{-3} s^{-1}	38
3	Ag	Coral-like dendrite	1.0×10^{-4} M	0.037 nmol	5.19×10^{-3} s^{-1}	39
4	Au	Spongy	1.03×10^{-4} M	0.03 nmol	2.1×10^{-3} s^{-1}	40
5	Al_2O_3/Pd	Nanowires	30×10^{-4} M	5.0×10^{-3} nmol	8.3×10^{-3} s^{-1}	41
6	Fe_3O_4@C@PtPd	Satellites–core	0.50×10^{-4} M	1.68 nmol	20.2×10^{-3} s^{-1}	42
7	$CoMn_2O_4$	Hierarchical microsphere	1.0×10^{-4} M	6.0×10^{-4} nmol	14.95×10^{-3} s^{-1}	This work

p-nitrophenol with respect to time were determined for cycle times. The values of k_{app} were evaluated for different cycles using slope values from the plots, $\ln(C_t/C_0)$ *vs.* time (C_t and C_0 are *p*-nitrophenol concentrations at time t and 0, respectively) (Fig. 5). As shown in Fig. 5, there is a linear relationship between $\ln(C_t/C_0)$ and reaction time (t) in the reduction reaction catalyzed by $CoMn_2O_4$ hierarchical microspheres (C400, C500, C600 and C700), which suggests that the reaction follows first-order kinetics. Table 4 shows the reaction rate constant of each catalytic reaction with different catalysts. According to the rate constant, with the increase of cycle times, the four catalysts show different features. In the four groups of cycle experiments, the rate constant inclined to a stability constant after being reused six times, except for the C700 where the rate constant gradually decreased as compared to the fresh catalyst, it no longer exhibits catalytic activity after four cycles. One of the reasons is reaction product poisoning. This is a common phenomenon in catalytic experiments. Another cause of the decrease may be associated with the hydrolysis of sodium borohydride. As shown in Fig. 4, compared with the other three samples (C400, C500 and C600), C700 takes the longest time for transforming *p*-nitrophenol to *p*-aminophenol. The whole process took about 7 min, almost twice the other three groups. During this period, hydrolysis of $NaBH_4$ was going on. Therefore, the concentration of $NaBH_4$ had greatly reduced after each cycle, and $NaBH_4$ plays an important role in the catalytic reduction of *p*-nitrophenol to *p*-aminophenol. So as the reaction time increases, the reaction rate decreased gradually. The same trend did not appear in the cycle experiment of the other three groups (C400, C500 and C600). Among the three groups, the rate constants of this catalytic reaction increased at first and then become stable with the increasing time of the catalytic reduction cycle. This phenomenon was probably correlated with the hydrolysis of $NaBH_4$.

Since the reaction involved using a large amount of $NaBH_4$, a strong reducing environment, the stability of the oxide during the reaction should be monitored carefully. C500 was selected to check the stability. After recycling 6 times, the reaction mixture was separated into two phases, the organic phase (excess $NaBH_4$

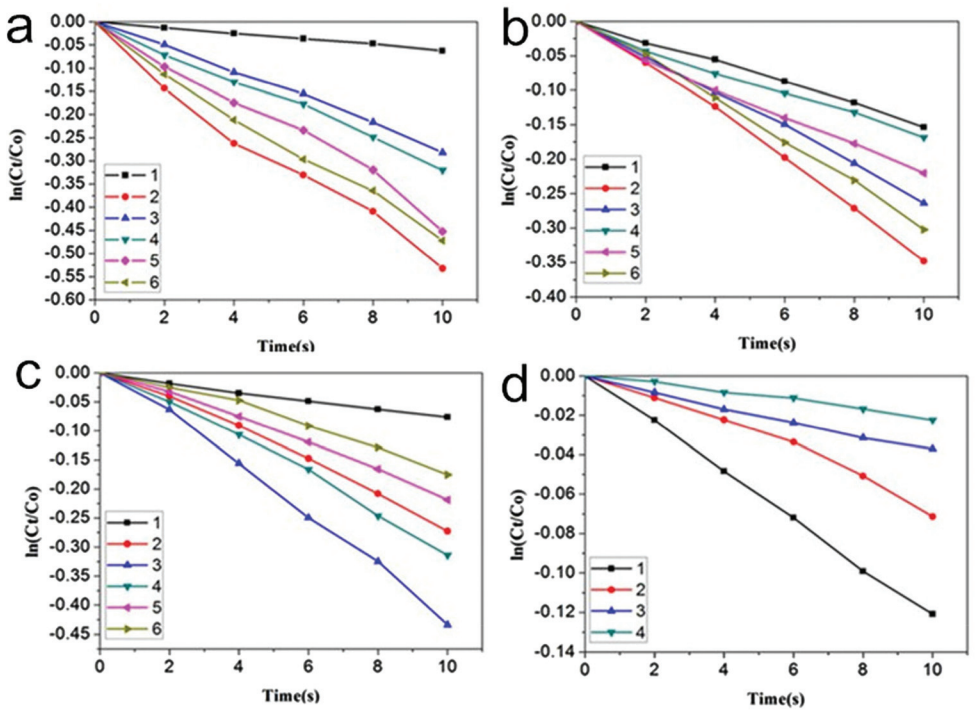

Fig. 5 Plots of ln(Ct/Co) *vs.* time for reduction catalyzed by recycled $CoMn_2O_4$ hierarchical microspheres: (a) C400, (b) C500, (c) C600, (d) C700 at room temperature (18 °C).

Table 4 Summary of rate constants for *p*-nitrophenol reduction catalyzed by recycling used $CoMn_2O_4$ hierarchical microspheres

Sample	k_{app} of first cycle (s^{-1})	k_{app} of second cycle (s^{-1})	k_{app} of third cycle (s^{-1})	k_{app} of fourth cycle (s^{-1})	k_{app} of fifth cycle (s^{-1})	k_{app} of sixth cycle (s^{-1})
C400	8.13×10^{-3}	54.16×10^{-3}	27.36×10^{-3}	30.74×10^{-3}	46.35×10^{-3}	46.49×10^{-3}
C500	14.95×10^{-3}	33.87×10^{-3}	25.92×10^{-3}	16.44×10^{-3}	22.62×10^{-3}	29.36×10^{-3}
C600	12.15×10^{-3}	24.35×10^{-3}	40.39×10^{-3}	25.99×10^{-3}	21.87×10^{-3}	20.87×10^{-3}
C700	7.42×10^{-3}	6.52×10^{-3}	2.88×10^{-3}	2.110×10^{-3}		

and *p*-aminophenol) and the C500 (C500-A). C500-A was collected after washing with absolute ethanol and deionized water, and then dried in an oven at 60 °C. The crystallographic structure of C500-A was analyzed by XRD. Fig. S3† shows no obvious change in the catalyst phase and the structure, compared with C500. All the peaks of C500-A correspond well to C500. For further investigation of the stability of C500, the XPS of C500-A was also performed (Fig. 6). According to the result, Co and Mn elements exist as Co^{2+}, Co^{3+}, Mn^{2+} and Mn^{3+} in both C500 and C500-A. The peak positions of C500 and C500-A are similar, which indicates that the valence of Co and Mn element did not change during the reaction. The above analysis shows that C500 has good stability during the reaction, suggesting that $CoMn_2O_4$ can be used as the catalyst in the reduction of *p*-nitrophenol to *p*-aminophenol.

A possible catalytic mechanism of the reduction of *p*-nitrophenol was proposed as follows. As evidenced from the basic steps included in the mechanism, the reduction reaction requires electron transfer from the donor BH_4^- ion. In the presence of $CoMn_2O_4$ hierarchical microspheres, it is understood that the steps include: (1) chemisorption of BH_4^- on the surface of the metal oxide[43,44] and followed by (2) transferring of electrons from BH_4^- to $CoMn_2O_4$ and then to the acceptor. The medium water is a polar protic solvent, which offers the required H^+ ions for the completion of the reduction reaction.[12] In this case, a good "electrical" connection between the particles will play an important role as the electrons have to be transported from the oxidation site to the reduction site.[45] According to previous reports, the spinel oxide can accelerate the process of liberation of hydrogen by the hydrolysis reaction of $NaBH_4$ and water.[22] And the hydrolysis of $NaBH_4$

$$NaBH_4 + 4H_2O \rightarrow NaOH + H_3BO_3 + 4H_2$$

produced small amounts of hydrogen;[46] many attempts have been made to hasten up the process for higher hydrogen generation.[47] Spontaneous liberation of hydrogen under visible light over spinel oxides of the general formula CuM_2O_4 (M = Al, Cr, Mn, Fe, Co) was encountered by Saadi *et al.*[18] Similarly, the increase in H_2 yield from aqueous $NaBH_4$ in the presence of Pt–TiO_2, Pt–CoO and Pt–$LiCoO_2$ was noticed by Kojima *et al.*[48] Hence, it could be presumed that the presence of the mixed metal spinel oxide leads to spontaneous *in situ* generation of hydrogen which in turn reduces *p*-nitrophenol rapidly.[22] $CoMn_2O_4$ hierarchical microspheres used in this report are a typical kind of spinel oxide, which can accelerate the process of the transforming *p*-nitrophenol to *p*-aminophenol in the same way. Importantly, the metal oxides possessing 'd^7' (Co element) and 'd^5' (Mn element) electronic configurations are active in the reduction of *p*-nitrophenol to *p*-aminophenol,[21] and they can induce the catalytic reduction by relaying electrons from the donor BH_4^- ions to the acceptor once they get adsorbed on the metal oxide surface. On the other hand, *p*-nitrophenolate ions were adsorbed by $CoMn_2O_4$ *via* physical adsorption. Hence, it can accelerate the process of the transforming *p*-nitrophenol to *p*-aminophenol on a large scale. The hierarchical microspheres assembled with nanosheets can ensure that every nanosheet participates in the reduction. The *p*-nitrophenolate ions and BH_4^- were fixed around the $CoMn_2O_4$ due to the cage effect, thereby the intermolecular collision increased, which makes the reduction reaction easier.[49]

For comparison, $CoMn_2O_4$ with non-hierarchical shape has been prepared by the chemical co-deposition method (Fig. S4†). The SEM (Fig. S4(a)†) showed $CoMn_2O_4$ with non-hierarchical shape. As shown in Fig. S4(c),† the whole catalytic process took about 10.5 min ($k_{app} = 1.05 \times 10^{-3}$), showing an activity even lower than that of the sample C700 (7.0 min, $k_{app} = 7.42 \times 10^{-3}$). This is because every nanosheet in a $CoMn_2O_4$ hierarchical microsphere can provide active sites, while only the surface active sites can catalyze the reduction of the $CoMn_2O_4$ particles with non-hierarchical shape, which leads to $CoMn_2O_4$ hierarchical microspheres assembled by nanosheets being more active.

As shown in Table 1, C500 showed the best catalytic performance among the four groups. The XRD indicated that neither crystallinity nor crystal size was the only factor that determines the catalytic effect of $CoMn_2O_4$ hierarchical microspheres, because C700 with the highest crystallinity showed the lowest catalytic performance, while C400 with the smallest crystal size also displays a poorer activity than C500. However, the XPS provides us some important information, $CoMn_2O_4$ hierarchical microspheres calcining at different temperatures

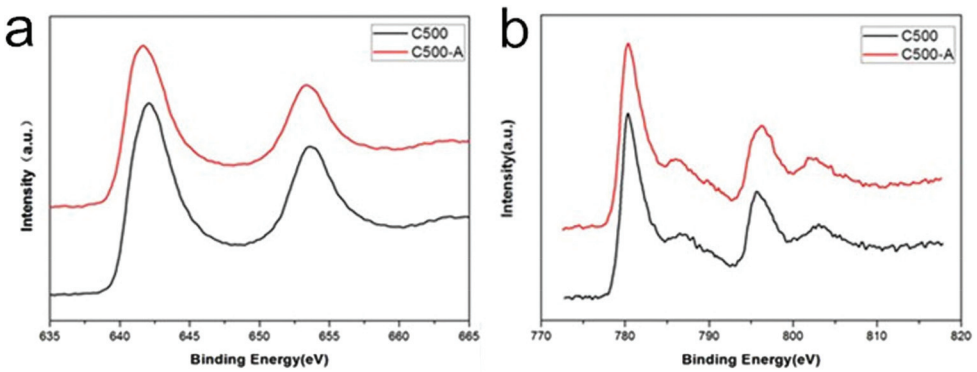

Fig. 6 XPS survey spectra of C500 and C500-A: (a) Co 2p, (b) Mn 2p.

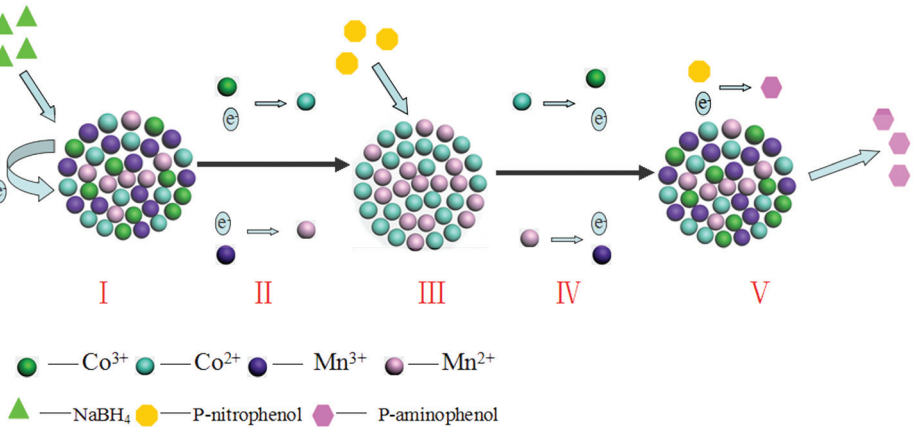

Scheme 1 Possible mechanism of the catalytic reduction of *p*-nitrophenol: (I) Adsorption of BH_4^- on the catalysts' surface, providing electrons to the catalyst. (II) Mn^{3+} and Co^{3+} accept these electrons to form Mn^{2+} and Co^{2+}. (III) Adsorption of *p*-nitrophenol on the catalysts' surface. (IV) Mn^{2+} and Co^{2+} donate their electrons to *p*-nitrophenol and being translated into Mn^{3+} and Co^{3+}. (V) *p*-Nitrophenol molecules accept electrons to generate *p*-aminophenol, *p*-aminophenol molecules desorb from the catalyst finally.

(C400, C500, C600 and C700) all contain the redox couples Co^{3+}/Co^{2+} and Mn^{3+}/Mn^{2+}, we can get $CoMn_2O_4$ hierarchical microspheres with different ratios of Mn^{3+}/Mn^{2+} and without altering the ratios of Co^{3+}/Co^{2+} by changing the thermal decomposition temperature. As is known, electron transfer was important for the catalytic reaction. The redox couples Co^{3+}/Co^{2+} and Mn^{3+}/Mn^{2+} can be expected to facilitate the oxide's role as an electron relay system that opens up pathways for diverse intermediate steps in the reaction of adsorbed species. Co^{3+} and Mn^{3+} tend to accept electrons at first and then transmit electrons through the action of Co^{2+} and Mn^{2+}. It is therefore suggested that the synergy effect between these metal ions improves the catalytic effect. With the changing of the ratio of Mn^{3+}/Mn^{2+}, the electronic acceptance and transmission rate was changing at the same time. Only when these two reached an equilibrium which takes place at the same rate, the $CoMn_2O_4$ hierarchical microspheres had the best catalytic effect. The proposed mechanism process is shown in Scheme 1. Thus another reason for the highest catalytic performance of C500 may be the appropriate ratio of Mn^{3+}/Mn^{2+} (1.15 : 1). At this ratio, the two redox couples Co^{3+}/Co^{2+} and Mn^{3+}/Mn^{2+} show the best synergy effect, leading to the highest catalytic performance of C500.

Conclusion

In the present study, we first report the high catalytic activity of $CoMn_2O_4$. The $CoMn_2O_4$ catalysts showed much higher activity than many noble metal catalysts, and the cycle rate constants for the $CoMn_2O_4$ catalysts (C400, C500, C600) showed good reusability of these catalysts. The special morphology and presence of active metal oxides with 'd^7' (Co element) and 'd^5' (Mn element) contribute positively to the catalytic reaction. Moreover, we found that 500 °C was the most appropriate thermal decomposition temperature at which we can get $CoMn_2O_4$ hierarchical microspheres with the highest catalytic performance, because an appropriate proportion of Mn^{3+}/Mn^{2+} was generated in the sample. Because of the reduced amount of catalyst as well as the good reusability, it is reasonable to suggest that $CoMn_2O_4$ catalysts have the potential to be used in industrial catalysis.

Acknowledgements

This work was supported by the National Natural Science Foundation (grants 21271163 and U1232211).

References

1 Y. Lu, Y. Mei and M. Ballauff, *J. Phys. Chem. B*, 2006, **110**, 3930.
2 C. V. Rode, M. J. Vaidya, R. Jaganathan and R. V. Chaudhari, *Chem. Eng. Sci.*, 2001, **56**, 1299.
3 M. J. Vaidya, S. M. Kulkarni and R. V. Chaudhari, *Org. Process Res. Dev.*, 2003, **7**, 202.
4 J. F. Corbett, *Dyes Pigm.*, 1999, **41**, 127.
5 C. V. Rode, M. J. Vaidya and R. V. Chaudhari, *Org. Process Res. Dev.*, 1999, **3**, 465.
6 S. Saha, A. Pal, S. Kundu, S. Basu and T. Pal, *Langmuir*, 2010, **26**, 2885.
7 Y. Mei, G. Sharma, Y. Lu and M. Ballauff, *Langmuir*, 2005, **21**, 12229.
8 M. M. Telkar, C. V. Rode, R. V. Chaudhari, S. S. Joshi and A. M. Nalawade, *Appl. Catal., A*, 2004, **273**, 11.
9 Y. C. Liu and Y. W. Chen, *Ind. Eng. Chem. Res.*, 2006, **45**, 2973.
10 G. J. Hutchings, *Catal. Today*, 2005, **100**, 55.
11 S. Arora, P. Kapoor and M. L. Singla, *React. Kinet. Mech. Catal.*, 2010, **99**, 157.
12 T. Yu, J. Zeng, B. Lim and Y. Xia, *Adv. Mater.*, 2010, **22**, 5188.

13 Y. Wu, T. Zhang, Z. Zheng, X. Ding and Y. Peng, *Mater. Res. Bull.*, 2010, **45**, 513.
14 D. Jana, A. Dandapat and G. De, *Langmuir*, 2010, **26**, 12177.
15 B. K. Min and C. M. Friend, *Chem. Rev.*, 2007, **107**, 2709.
16 Z. Y. Zhang, C. L. Shao, P. Zou, P. Zhang and M. Y. Zhang, *Chem. Commun.*, 2011, **47**, 3906.
17 X. K. Kong, Z. Y. Sun, M. Chen, C. L. Chen and Q. W. Chen, *Energy Environ. Sci.*, 2013, **6**, 3260.
18 X. K. Kong, C. L. Chen and Q. W. Chen, *Chem. Soc. Rev.*, 2014, **43**, 2841.
19 A. L. Wang, H. B. Yin, H. H. Lu, J. J. Xue, M. Ren and T. S. Jiang, *Catal. Commun.*, 2009, **10**, 2060.
20 A. K. Patra, A. Dutta and A. Bhaumik, *Catal. Commun.*, 2010, **11**, 651.
21 T. R. Mandlimath and B. Gopal, *J. Mol. Catal. A: Chem.*, 2011, **350**, 9.
22 T. Swathi and G. Buvaneswari, *Mater. Lett.*, 2008, **62**, 3900.
23 S. Saadi, A. Bouguelia and M. Trari, *Renew. Energy*, 2006, **31**, 2245.
24 I. O. Ali, *J. Therm. Anal. Calorim.*, 2014, **116**, 805.
25 T. Mathew, S. M. Shylesh, B. Devassy, M. Vijayaraj, C. V. V. Satyanarayana, B. S. Rao and C. S. Gopinath, *Appl. Catal., A*, 2004, **273**, 35.
26 A. K. Neyestanakl and L. E. Lindfors, *Combust. Sci. Technol.*, 1994, **97**, 121.
27 L. Hu, H. Zhong, X. R. Zheng, Y. M. Huang, P. Zhang and Q. W. Chen, *Sci. Rep.*, 2012, **2**, 986.
28 P. Mahata, D. Sarma, C. Madhu, A. Sundaresen and S. Natarajan, *Dalton Trans.*, 2011, **40**, 1952.
29 A. V. Salker and S. M. Gurav, *J. Mater. Sci.*, 2000, **35**, 4713.
30 N. R. Jana, Z. L. Wang and T. Pal, *Langmuir*, 2000, **16**, 2457.
31 X. W. Lou, D. Deng, J. Y. Lee and L. A. Archer, *J. Mater. Chem.*, 2008, **18**, 4397.
32 C. Wang, D. L. Wang, Q. W. Wang and L. Wang, *Electrochim. Acta*, 2010, **55**, 6420.
33 S. W. Oh, H. J. Bang, Y. C. Bae and Y. K. Sun, *J. Power Sources*, 2007, **173**, 502.
34 N. Yan, L. Hu, Y. Li, Y. Wang, H. Zhong, X. Y. Hu, X. K. Kong and Q. W. Chen, *J. Phys. Chem. C*, 2012, **116**, 7227.
35 B. J. Tan, K. J. Klabunde and P. M. A. Sherwood, *J. Am. Chem. Soc.*, 1991, **113**, 855.
36 S. Praharaj, S. Nath, S. K. Ghosh, S. Kundu and T. Pal, *Langmuir*, 2004, **20**, 9889.
37 X. Lu, X. Bian, G. Nie, C. Zhang, C. Wang and Y. Wei, *J. Mater. Chem.*, 2012, **22**, 12723.
38 Z. Jin, M. Xiao, Z. Bao, P. Wang and J. Wang, *Angew. Chem., Int. Ed.*, 2012, **51**, 6406.
39 M. H. Rashid and T. K. Mandal, *J. Phys. Chem. C*, 2007, **111**, 16750.
40 M. H. Rashid, R. R. Bhattacharjee, A. Kotal and T. K. Mandal, *Langmuir*, 2006, **22**, 7141.
41 R. Li, P. Zhang, Y. M. Huang, C. L. Chen and Q. W. Chen, *Appl. Mater. Interfaces*, 2013, **5**, 12695.
42 P. Zhang, R. Li, Y. M. Huang and Q. W. Chen, *Appl. Mater. Interfaces*, 2014, **6**, 2671.
43 Y. Kojima, K. Suzuki, K. Fukumoto, M. Sasaki, T. Yamamoto, Y. Kawai and H. Hayashi, *Int. J. Hydrogen Energy*, 2002, **27**, 1029.
44 R. Fernandes, N. Patel, A. Miotello and M. Filippi, *J. Mol. Catal. A: Chem.*, 2009, **298**, 1.
45 J. Zeng, Q. Zhang, J. Y. Chen and Y. N. Xia, *Nano Lett.*, 2010, **10**, 30.
46 R. Aiello, J. H. Sharp and M. A. Matthews, *Int. J. Hydrogen Energy*, 1999, **24**, 1123.
47 V. C. Y. Kong, F. R. Foulkes, D. W. Kirk and J. T. Hinatsu, *Int. J. Hydrogen Energy*, 1999, **24**, 665.
48 Y. Kojima, Y. Kawai, H. Nakanishi and S. Matsumoto, *J. Power Sources*, 2004, **135**, 36.
49 Z. F. Jiang, J. M. Xie, D. L. Jiang, J. J. Jing and H. R. Qin, *CrystEngComm*, 2012, **14**, 4601.